“Application of Immersed Boundary Methods for physiological flow analysis in 2D stenosed artery”

A Dissertation

SUBMITTED IN PARTIAL FULFILLMENT OF REQUIREMENTS

FOR AWARD OF DEGREE OF

Master of Engineering

in

Thermal Engineering

Submitted by:

Gurpreet Singh

RegistrationNumber: 801683014

Under the Supervision of:

Dr. Neeraj Kumar

Assistant Professor, MED

Dr. Manish Kumar

Assistant Professor, MED

Mechanical Engineering Department

Thapar Institute of Engineering & Technology

Patiala-147003

Punjab

CERTIFICATE

I hereby declare that the thesis entitled, **"Application of Immersed Boundary Methods for physiological flow analysis in 2D stenosed artery "** is an authentic record of my work carried out as per requirements for the award of degree of **Master of Engineering** in **Thermal Engineering** at **Thapar Institute of Engineering & Technology, Patiala** under the supervision of **Dr. Neeraj Kumar**, Assistant Professor, Mechanical Engineering Department, Thapar Institute of Engineering & Technology, Patiala and **Dr. Manish Kumar**, Assistant Professor, Mechanical Engineering Department, Thapar Institute of Engineering & Technology, Patiala during June 2016 to June 2018. No part of the matter embodied in this report has been submitted to any other university or institute for the award of any other degree.

Date 21|08|2018

Gurpreet Singh

It is certified that the above statement made by the student is correct to the best of my knowledge and belief.

Dr. Neeraj Kumar
Assistant Professor
Mechanical Engineering Department
T.I.E.T
Patiala-147004

Dr. Manish Kumar
Assistant Professor
Mechanical Engineering Department
T.I.E.T
Patiala-147004

ACKNOWLEDGEMENT

I would like to thank my supervisors: Dr. Neeraj Kumar, Assistant Professor, M.E.D., T.I.E.T, Patiala, and Dr. Manish Kumar, Assistant Professor, M.E.D., T.I.E.T, Patiala, for their continous guidance and support to my research. I am grateful to them for their encouragement and patience in overcoming numerous obstacles I have been facing through my thesis. There were times when things seemed tough and undoable, but they guided me through those times with extreme patience and perseverence. I am grateful to them for introducing me to the world of computational fluid dynamics.

I would also like to express special thanks to Rishabh P. Sharma, for teaching me how to work in unix, during the start of my thesis.

Last but not the least, I would like express my gratitude to my family and my friends for supporting me spiritually throughout the course of my Master's.

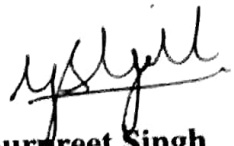

Gurpreet Singh

ABSTRACT

In this dissertation, numerical analysis of blood flow in a two dimensional constricted artery channel with the help of Immersed Boundary Method (IBM) is demonstrated for both steady and unsteady flow condtions. SOLA technique, which is based on FDM, is employed to solve the fluid flow equations and IBM is used to track and interpolate boundary conditions at the curved boundary. The IBM used in this work is similar to that of Kumar et al. [1]. The two dimensional constricted artery channel mimics the model of canine femoral artery used by Daly [2]. The fluid properties are also similar to that of canine blood. The steady flow analysis is performed using a Reynolds number of 293.43, which corresponds to the average velocity of the pulsatile flow published by McDonald [3]. For unsteady flow analysis, the physiological flow of canine femoral artery published by McDonald [3] is used directly. Both studies have been performed for various constriction sizes.

Results from the numerical simulation reveal that the length of flow reversal zone and the wall shear stress are directly proportional to the degree of occlusion in the arterial channel for both steady and unsteady flow. These factors can further lead to an agressive plaque deposition in a real artery which can worsen the ailment for a diseased person. The results of the study have medical significance as it could predict the threshold for surgical intervention.

Keywords: IBM; Stenosis; SOLA; Arterial flow.

Contents

List of Figures iv

List of Tables v

Nomenclature vi

Abbreviations vii

1 Introduction 1

1.1 Introduction 1

1.2 Literature Survey 2

1.3 Gaps Identified 6

1.4 Objective of the present study 6

1.5 Thesis Outline 6

2 Methodology 7

2.1 SOLA solver 7

2.2 Immersed Boundary Method 9

2.3 Boundary Conditions 11

2.4 Proposed Algorithm 13

2.5 Constriction model and fluid properties 14

3 Comparative Study 15

3.1 Steady channel flow 15

3.2 Backward Step flow 17

4 Steady Flow Simulation 19

4.1 Short constriction length ($5r_0$) 19

4.2 Long constriction length ($10r_0$) 22

4.3 Conclusions 23

5 Unsteady Flow Simulation 25

6 Conclusions **29**

6.1 Scope for future work 29

List of Figures

1.1 Velocity Profiles at various Womerseley Number 3

2.1 SOLA solver computaional domain with velocity and pressure representation for a cell 7

2.2 Representation of the parameters and the grids with respect to the master grid: a) Position of parameters (pressure, horizontal velocity and vertical velocity) within a discretized cell; b) Presure grid vs Master grid; c) Horizontal velocity grid vs Master grid; and d) Vertical velocity grid vs Master grid 10

2.3 Boundary Conditions interpolation at the interface nodes 11

2.4 Inlet horizontal velocity profiles for: a) Channel flow; b) Backward step flow . 12

2.5 Constricted Channel 14

3.1 Offset in rectangular channel for the appliacation of IBM 15

3.2 Variation of horizontal velocity with channel depth at offset of 0.25dy 16

3.3 Variation of horizontal velocity with channel depth at offset of 0.75dy 16

3.4 Comparison of horizontal velocity at x=7 and x=15 17

3.5 Comparison of wall shear stress at bottom and top wall 17

3.6 Comparison of wall pressure at bottom and top wall 18

4.1 Offset in the constriction model 19

4.2 Velocity profiles for $2z_0=5r_0$ (The four different positions are taken with respect to the start of stenosis or constriction) 20

4.3 WSS for $2z_0=5r_0$(Wall length starts from $2r_0$ before constriction and ends at $2r_0$ after constriction) 21

4.4 Pressure contours and streamline for: a) 25% Constriction; b) 50% Constriction; and c) 75% Constriction. 21

4.5 Velocity profiles for $2z_0=10r_0$ 22

4.6 WSS for $2z_0=10r_0$(Wall length starts from $2r_0$ before constriction and ends at $2r_0$ after constriction) 23

4.7 Pressure contours and streamline for: a) 25% Constriction; b) 50% Constriction; and c) 75% Constriction 23

5.1 Mean velocity in canine femoral artery for a cardiac cycle 25
5.2 Horizontal velocity at various constrictions and at various time steps at the center of constriction. 26
5.3 Wall shear stress at various constrictions and at various time steps along the wall length (Wall length starts from $2r_0$ before constriction and ends at $2r_0$ after constriction) 27
5.4 Variation of phase lag with Womerseley number. 27
5.5 Pressure contours and streamline at: a) t= $0.2T_0$; b) t= $0.4T_0$; c) t= $0.6T_0$; d) t= $0.8T_0$; and e) t= T_0 28

List of Tables

3.1 RMSE for channel flow simulation 16
3.2 Size of lower and upper recirculation zone 18

Nomenclature

D	Channel depth
f	Body force
h	Constriction depth
n	Normal distance
r	Channel half depth
R_e	Reynolds number
U_{in}	Inlet velocity
ν	Kinematic viscosity

Abbreviations

ALE Arbitrary Lagrangian-Eulerian.

CFL Courant Frederic Lewy.

FDM Finite Difference Method.

FEM Finite Element Method.

FFT Fast Fourier Transforms.

FSI Fluid-Structure Model.

FVM Finite Volume Method.

IBM Immersed Boundary Method.

MAC Marker and Cell.

MPI Message Passing Interface.

NIM Nodal Integral Method.

RCR Resistance Capacitance Resistance.

RMSE Root Mean Square Error.

SIMPLE Semi-Implicit Method for Pressure Linked Equations.

SOLA Solution Algorithm.

TDMA Tri-diagonal Matrix Algorithm.

Chapter 1

Introduction

1.1 Introduction

The physiological flow in arteries has been under study for well over six decades. Incepted by Womersley in 1954 [4] with his popular research on flow across a pipe with a pulsating pressure difference, it has now reached a level where researchers have developed dedicated packages for real time simulation of the blood flow in complex arterial geometry. They can then even verify the simulation results with the help of prosthetics developed by 3D printers.

Stenosis or arterial constriction occurs due to the deposition of plaque (cholesterol and lipid substances) on the inner surface of the blood vessel called lumen. Sako [5] studied the effect of turbulence and hypertension on experimental atherosclerosis. He established that the increase in physical factors such as turbulence, increased flow, and hypertension worsens atherosclerosis. Later Fry [6] studied the effects of subjecting the endothelial surface to high wall shear stress. He found that continous exposure of the lumen to a shear stress in excess of 38 ± 7.5 Pa can cause a marked deteoriation in the endothelial layer.

Considering this many researchers have then worked on analyzing the blood flow through a constriction or stenosis. Young and Forrester [7] were the first to investigate this and found the length of the post-stenotic flow separation region using numerical analysis for steady flow. Later, Young and Tsai [8, 9] performed experimental analysis for both steady and pulsatile flow through a stenotic polyester tube using distilled water to establish an experimental results basis for further theoretical computations. Then Daly [2, 10] performed numerical analysis of pulsatile flow through constricted arteries for rigid and distensible wall using ALE procedure using the blood flow data of provided by McDonald [3]. He found that phase and amplitude of pressure gradient are sensitive indicators for pregression of atheromateous lesion in a stenosed artery. Vanderschuren et al. [11] applied the FEM technique to study the flow through stenosis for various degrees of occlusion for steady and pulsatile flow. Moayeri and Zendehbudi [12] applied the SIMPLER algorithm along with coordinate transformation to compare the results of pulsatile flow thorough a stenosis for a simple pulsatile flow with the physiological flow.

Vignon and Taylor [13] used the coupled multi-domain method to implement the boundary conditions that accomodate the downstream arterial models. They used a variety of boundary conditions for different outlets such as resistive, impedance, transient wave theory, RCR, etc.

Most of the numerical study of physiological flow in the complex arterial geometry has been performed using either the unstructured mesh generation methods or some form of boundary mapping tehnique. This process is generally temporally and computationally expensive for moving boundaries as the domain has to remeshed after each time step. The use of IBM simplifies this process as the computation is performed on a body non-conformal grid. A search algorithm is used for tracking the solid-fluid interface and the boundary conditions are interpolated for the cartesian points which are adjacent to the boundary and inside the fluid domain.

Peskin [14] was the first to use IBM to simulate flow around a heart valve. He modified the governing equations using appropriate forcing terms to incorporate the boundary effects. Overtime several variants of IBM have deen developed for various problems like biological flows, structural mechanics, flow over over curved bodies, etc. This has been discussed in detail by Mittal and Iaccarino [15].

In the current work, SOLA solver developed by Hirt et al. [16] is used to solve steady and transient flow in a constricted domain. The constricted domain has a curved profile which is guided by a cosine equation. IBM is used to implement the Dirichlet boundary conditions for the curved domain. Also, comparative studies have been made for channel flow and backward step flow to test the validity of the solving scheme.

1.2 Literature Survey

Various researchers have worked on solving physioligical flow in arteries. Their work has been summarized below.

1. **Womersley [4]** was the first to formulate flow in a pipe with a pulsating pressure difference. He derived the equation of flow and velocity using a pulsatile differential pressure source and found that a phase difference exists between the pressure pulse and flow pulse. The physiological flow in arteries is generally in the laminar range (Re$<$2000), so the nature of flow has to be determined from some other parameter. He introduced a very important parameter known as Womerseley number, α ($= \mathrm{R}\sqrt{\omega/\nu}$) for this purpose. He found that the nature of pulsatile flow ranges from parabolic ($\alpha < 1$) to womerseley($1 < \alpha < 10$) to plug ($\alpha > 10$) as shown in figure 1.1:

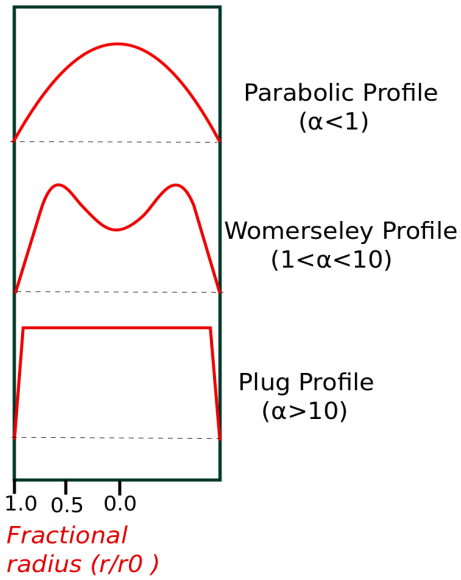

Figure 1.1: Velocity Profiles at various Womerseley Number

2. **Merrill and Pelletier [17]** performed rheological study of human blood to observe the transition from Newtonian to non-Newtonian nature. They found that blood is essentially a Non- Newtonian fluid but the non-Newtonian characteristics of blood are apparent only at low rates of shear, and that for shear rates above 100 sec^{-1}, blood can be considered to be a Newtonian fluid. So generally in most of the studies blood is considered as a Newtonian fluid. This study is an important basis for scientists who conduct their study considering blood as a Newtonian fluid.

3. **Young and Forrester [7]** developed the solution for a two dimensional steady flow in a converging diverging tube. He assumed the blood to be Newtonian, homogenous and incompressible fluid. He found that steady flow solution have relevance for physiological flow where $\alpha << 1$. He made some significant transformations in the momentum equations to simplify the computation. He observed that a small recirculation zone exists for a Reynolds number of 150. Also he found that the existence of a positive pressure gradient does not necessarily imply that separation will occur. The profile gradient (dR/dZ) required for flow separation to occur is approximately four times greater than its value for the development of an adverse pressure gradient.

4. **Young and Tsai [8]** performed experimental analysis for steady flow through both the axisymmetric and non-axisymmetric stenosis using in-vitro models. The fluid used was distilled water and the tube was made of polyester resin. Aniline blue dye was injected

to track the fluid and to determine the separation and reattachment points. They observed that at higher critical Reynolds number, the velocity began to fluctuate significantly with time, and the flow transitioned to turbulent. The pressure drop was found to be higher than the pressure drop of Poiseuille analytical solution. Also the pressure drop did not follow a linear relation with increase in Reynolds number as was the case with Poiseuille solution. Their overall conclusion was that qualitatively, the characteristics of the general flow are independent of shape but specific quantitative information is dependent on both size and shape.

5. **Daly [10]** performed the simulation for transient flow through a two dimensional stenosed artery. He applied the ALE method to accomodate the distensibility of the artery. For the simulation he used the flow of the canine femoral artery given by Mcdonald [3] at the inlet and a zero pressure gradient at the outlet. He performed the study for three different degrees of area occlusion: 23% , 44% and 61%. He observed that for a small elastic modulus the elastic force does not begin to restore the wall until after the incoming fluid has begun to decelerate.

6. **Daly [2]** again employed the ALE method to study the pulsatile flow through artery but he did not take the distensibility of the arterial wall into account. He assumed that neglecting wall distensibilty did not affect the results severely as the attention of the study was confined to femoral artery only where the affect of wall distensibility is negligible. The geometric model and the flow model of the artery is based on the characteristics of canine femoral artery. He observed that the location of systolic and diastolic points of the separation and attachment relative to the apex of the stenosis did not change with the increase in constriction. He also observed that the existence of radial fow acceleration could be a factor in thrombus dislodgement if the radial acceleration gets out of phase with arterial motion.

7. **Vanderschuren et al. [11]** performed the study of pulsatile and steady flow through constricted artery using Galerkin FEM. In this technique the time-step is variable and is calculated using a predictor-corrector method. For steady flow, he obtained the results by varying not only the degree of occlusion but also the length of occlusion with various Reynold's number. For pulsatile flow, he varied the Womersely number. For steady flow, he observed that for flow with highest Reynold's number, most severe constriction and

least length, the value of wall shear stress was 55 times that of non- stenotic region. For pulsatile flow, he observed that maximum wall shear stress coincided with maximum velocity and it was slightly higher for smaller α.

8. **Moayeri and Zendehbudi [12]** compared the stenotic flow results of simple pulsatile (harmonic) flow with physiological flow. He employed the SIMPLER algorithm alongwith coordinate transformation for performing his numerical analysis. He reported significant difference in the wall shear stress values for the physiological flow compared to the simple harmonic flow. Also qualitatively, the streamline character was noticeably different in the two cases.

9. **Vignon and Taylor [13]** performed the simulation on complex arterial structure with numerous outlets and with different outflow boundary conditions for each of them. They employed the "coupled momentum method" to accomodate the transient outlet boundary conditions with the arterial flow solver. They observed that the spurious wave fluctuations disappear as the modes in Green's function becomes 50. For periodic case they observed that the impedance boundary condition is the most relevant boundary condition with regards to wave propagation. So, they concluded that the impedance boundary condition was best suited to accomodate the wave reflections naturally arising from downstream beds.

10. **Anupindi et al. [18]** employed the IBM on FVM solver to simulate flow in thoracic aortic aneurysm and abdominal aortic aneurysm. They also employed the multi-block grid approach to use the parallel paradigm. They observed that the thoracic aortic aneurysm simulations reveal complex vortical and unsteady flow fields. These results need to be considered in designing and implanting medical devices such as stent grafts.

11. **Kumar et al. [1]** simulated fluid flow for a moving boundary using IBM. They coupled the MAC and SOLA solvers for the transient flow solution over a curved moving body. They curbed the spurious pressure fluctuations generally reported in case of moving boundary while maintaining the simplicity of the solver. They also employed the "selective retagging" approach to reduce the computational overhead. They also demonstrated that the convergence rate of the hybrid MAC-SOLA solver is better than the conventional MAC solver.

1.3 Gaps Identified

1. Few studies on physiological flow on arterial flows have been carried out to relate flow structure and cardiovascular diseases. Research in this field is still in its infancy.

2. Intricate grid generation methods are involved which have to be regenerated continously in case of fluid structure problems. This can be eliminated using body non-conformal grid approach.

3. Implementation of body conformal grid in a complex geometry such as a stenosed artery is always a challenging task.

1.4 Objective of the present study

1. To study the implementation of IBM over complex boundaries while maintaining the simplicity of the SOLA solver.

2. To study steady flow through a constricted channel with varying degree of constriction and varying length of constriction.

3. To study pulsatile flow through a constricted channel with varying degree of constriction.

1.5 Thesis Outline

The detailed methodology of the solver is described in Chapter-2. The discretization schemes of the SOLA solver and the implementaion of boundary at the curved boundary using IBM are discussed in detail in this chapter. It also contains the Fourier transformation of the inlet pulsatile flow of canine femoral artery which is used for pulsatile flow simulation. In the Chapter-3, the solver is tested for channel flow and backward step flow. Comparative study and proximity of the numerical solution to the analytical solution is demonstrated in this chapter. In Chapter 4, results and discussion of the steady flow are included. Reynolds number used for steady flow is 293.3. The steady flow results are obtained for various degrees of occlusion and various lengths of stenosis. In Chapter 5, results and discussion of the pulsatile flow are included. The pulsatile flow results are for a Womerseley number of 3.43. The Reynolds number for the pulsatile flow varies from 0 to 2006.2. The degree of occlusion is varied for pulsatile flow. The last chapter contains the conclusion of the study and the scope for future work.

Chapter 2

Methodology

2.1 SOLA solver

The present study focusses on study of physiological flow simulation through a two dimensional curved channel. Hence, the governing equations of momentum and mass conservation of homogenous, Newtonian and incompressible flow on cartesian coordinates are used. The governing equations are as follows:

$$\frac{\partial V}{\partial t} + (V \cdot \nabla)V = -\nabla \cdot p + \nu \nabla^2 V + f \tag{2.1}$$

$$\nabla \cdot V = 0 \tag{2.2}$$

In the current work SOLA solver is used for solving the momentum equations. The solver is based on FDM. It uses the staggered grid approach with velocities defined on the forward face centres (i.e. horizontal velocity (u) at the right face centre and vertical velocity (v) at the top face centre) and the pressure (p) defined at the cell centre as shown in figure 2.1.

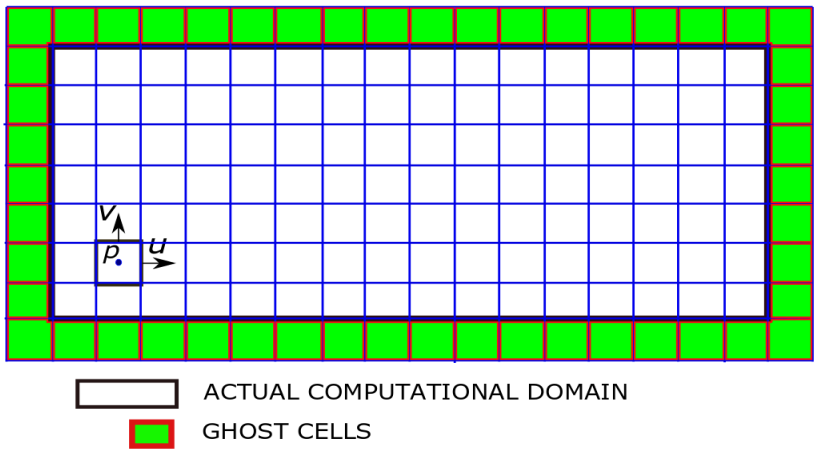

Figure 2.1: SOLA solver computaional domain with velocity and pressure representation for a cell

In this solver, initially the computational domain is divided into a finite number of rectangular

cells with an extra layer of ghost cells on all sides. The ghost cells are necessary for the staggered grid velocity and pessure representations but they are not part of the computation.

SOLA is purely an explicit method. It uses a two step approach to obtain the results at any given time step which is known as predictor corrector method. First, the results for n+1th time step are predicted from results at nth time step by using the following equation [19]:

$$\tilde{u}_{i,j}^{n+1} = u_{i,j}^{n} - \delta t \frac{(p_{i,j}^{n} - p_{i+1,j}^{n})}{\delta x} + (CONVU + \nu DIFFU)^{n} \delta t \tag{2.3a}$$

$$\tilde{v}_{i,j}^{n+1} = v_{i,j}^{n} - \delta t \frac{(p_{i,j}^{n} - p_{i,j+1}^{n})}{\delta y} + (CONVU + \nu DIFFU)^{n} \delta t \tag{2.3b}$$

Here "CONVU" and "DIFFU" represent the second order discretized forms of convective and diffusive terms in Navier Stokes equation.

Second, the obtained results are put through a corrector loop to obtain the final corrected velocity and pressure at the n+1th time step. In the corrector step, first the pressure correction term *p'*) for the velocity and pressure correction is computed from the given equation:

$$p'_{i,j} = -\omega \frac{(\nabla \cdot \tilde{V}^{n+1})_{i,j}}{2\delta t(\frac{1}{\delta x^2} + \frac{1}{\delta y^2})}, \tag{2.4}$$

where $\nabla \cdot \tilde{V}^{n+1}$ is the velocity divergence field for a particular cell. It is given by:

$$(\nabla \cdot \tilde{V}^{n+1})_{i,j} = \frac{\tilde{u}_{i,j}^{n+1} - \tilde{u}_{i-1,j}^{n+1}}{\delta x} + \frac{\tilde{v}_{i,j}^{n+1} - \tilde{v}_{i,j-1}^{n+1}}{\delta y} \tag{2.5}$$

Then the velocity and pressure are corrected iteratively using this pressure correction term until the velocity divergence field is reduced to the prescribed tolerance limit. The tolerance limit used for the current study is 10^{-5}. The correction equations are as given below:

$$u_{i,j}^{n+1} = \tilde{u}_{i,j}^{n+1} + \delta t \frac{p'_{i,j}}{\delta x} \tag{2.6a}$$

$$u_{i-1,j}^{n+1} = \tilde{u}_{i-1,j}^{n+1} - \delta t \frac{p'_{i,j}}{\delta x} \tag{2.6b}$$

$$v_{i,j}^{n+1} = \tilde{v}_{i,j}^{n+1} + \delta t \frac{p'_{i,j}}{\delta y} \tag{2.6c}$$

$$v_{i,j-1}^{n+1} = \tilde{v}_{i,j-1}^{n+1} - \delta t \frac{p'_{i,j}}{\delta y} \tag{2.6d}$$

$$p_{i,j}^{n+1} = \tilde{p}_{i,j}^{n+1} + p'_{i,j} \tag{2.6e}$$

The discretization scheme used for the temporal velocity and spatial pressure term is first order whereas the diffusive term is discretized using second order central difference scheme. The convective term is discretized using the second order upwind scheme of the FVM (2.7)[19].

$$u_{i+\frac{1}{2},j} = \frac{3}{2}u_{i,j} - \frac{1}{2}u_{i-1,j} \tag{2.7a}$$

$$v_{i,j+\frac{1}{2}} = \frac{3}{2}v_{i,j} - \frac{1}{2}v_{i,j-1} \tag{2.7b}$$

The second upwind convective scheme of FVM is chosen over second upwind convective scheme of FDM because it works better for cases which have higher Reynolds number such as backward step flow and channel flow with Reynolds number greater than 1000. However, the results of FDM convective scheme are reasonably appropriate for cases which have low Reynolds number such as lid driven cavity.

2.2 Immersed Boundary Method

The application of IBM consists of two major processes: a) tracking the solid fluid interface; and b) applying the boundary conditions for various parameters at the interface nodes using interpolation.

Tracking: The tracking of solid fluid interface is performed using an appropriate search method. In the present work, marker particle method is used for interface tracking. In this method, first the 2D profile is disintegrated into a finite number of segments. The size of the segment is kept half of the size of the discretized domain cell. Then the centroid ($C(x,y)$) and normal ($\hat{n}$) of each segment is obtained. Each node element (or discretized cell corner in present case) is assigned a particular profile segment which is closest to it. Then the position vector ($\vec{p}$) of the node from the assigned profile segment is obtained. The scalar multiplication of the position vector and the normal to profile segment i.e. $\vec{p}\cdot\hat{n}$ gives the normal distance (d_n) of the node from the profile element. If d_n is positive the node is tagged as fluid node and if d_n is negative the node is tagged as solid node. Similar procedure is followed for the the cell centre grid, cell top face centre grid and cell right face centre grid where the pressure, vertical velocity and horizontal velocity are defined respectively. A comparative representaion of the pressure,

vertical velocity and horizontal velocity grids with respect to the domain discretization grid or master grid is shown in figure 2.2.

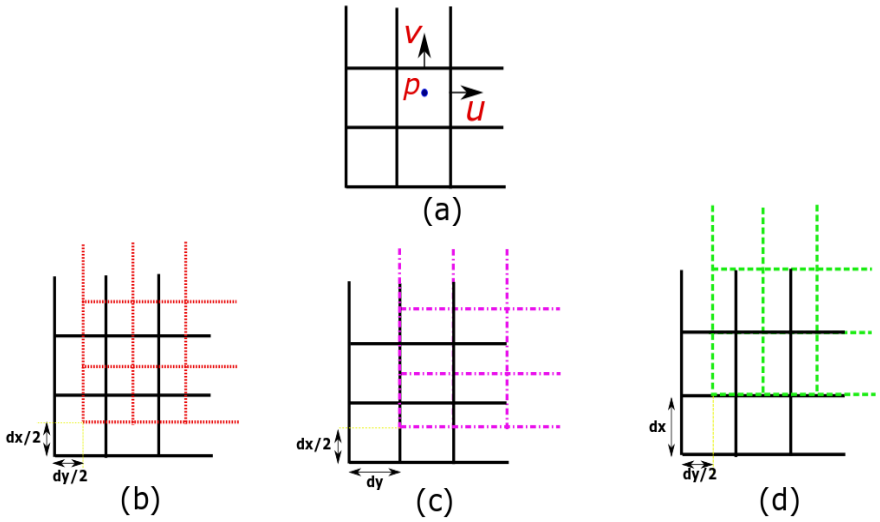

Figure 2.2: Representation of the parameters and the grids with respect to the master grid: a) Position of parameters (pressure, horizontal velocity and vertical velocity) within a discretized cell; b) Presure grid vs Master grid; c) Horizontal velocity grid vs Master grid; and d) Vertical velocity grid vs Master grid

Interpolating boundary conditions: To apply the boundary conditions at the interface nodes first the intercepted cells are identified. Then the four parameters of the intercepted cell namely horizontal velocity at right face centre, horizontal velocity at left face centre, vertical velocity at top face centre and vertical velocity at bottom face centre are calculated by using an appropriate forcing function. In the current study we have employed a quadratic forcing function for boundary condition application as given in the following equation:

$$F_n = an^2 + bn + c \tag{2.8}$$

Here n represents the normal distance from the boundary or interface.

For solving the quadratic function three values of the function at three distinct points are needed. The first is obtained by the boundary condition at the interface and the other two are obtained by first projecting normally into the fluid domain and then by interpolating linearly from the known values at fluid nodes as shown in figure 2.3.

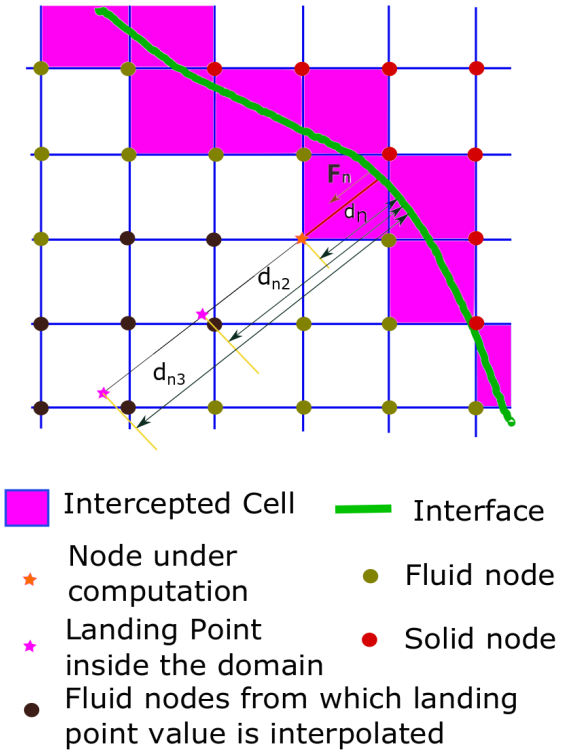

Figure 2.3: Boundary Conditions interpolation at the interface nodes

2.3 Boundary Conditions

The boundary conditions applied at the inlet, the wall and the oulet are given in the equation 2.9. The inlet has only horizontal velocity and no vertical velocity whereas the wall has no slip boundary condition. At the outlet zero velocity gradient is applied.

$$Inlet; \qquad u_{i,j} = U_{in}, \quad v_{i,j} = 0 \tag{2.9a}$$

$$Wall; \qquad V = 0 \tag{2.9b}$$

$$Outlet; \qquad \frac{\partial V}{\partial x} = 0 \tag{2.9c}$$

U_{in} is dependent upon the case under study. For channel flows, both constricted and straight, it has a rectilinear spatial profile whereas for backward step flow the spatial profile is divided into two parts: the bottom half has zero velocity as it corresponds to the wall and the top half has a parabolic spatial profile corresponding to the developed profile in the half channel for a Reynolds number of 800 as shown in figure 2.4

Temporally U_{in} remains same has a constant numeric value for the steady flow case and is calculated from the Reynolds number using the following equation:

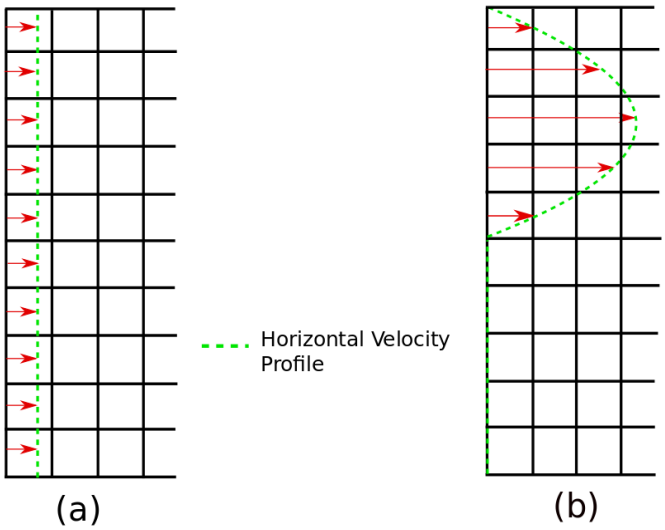

Figure 2.4: Inlet horizontal velocity profiles for: a) Channel flow; b) Backward step flow

$$U_{in} = \frac{R_e \nu}{2D} \tag{2.10}$$

Here D represents the depth of the channel.

However, for the transient flow, U_{in} is a function of time. This function could be a simple harmonic function in terms of sine or cosine or it could be derived from a set of data using FFT. Through FFT, a smooth function of sine and cosine terms is obtained through transformation of given data which replicates the given data as given in equation 2.11. The accuracy of the replication depends upon the number of modes (N) used in transformation.

$$f(t) = a_0 + \sum_{m=1}^{N} a_m cos(\frac{2\pi mt}{T}) + \sum_{n=1}^{N} b_n sin(\frac{2\pi nt}{T}) \tag{2.11}$$

where,

$$a_0 = \frac{1}{T}\int_0^T f(t)dt \tag{2.12a}$$

$$a_n = \frac{2}{T}\int_0^T f(t)cos(\frac{2\pi mt}{T})dt \tag{2.12b}$$

$$b_n = \frac{2}{T}\int_0^T f(t)sin(\frac{2\pi nt}{T})dt \tag{2.12c}$$

To simplify computation the inlet and outlet are aligned with the cartesian grid. IBM is applied only at the wall for the application of boundary conditions. It should be noted that pressure boundary conditions are not applied in the SOLA method. Only velocity boundary conditions have relevance in this solver.

2.4 Proposed Algorithm

The implementation algorithm for the proposed computational scheme can be summarized as:

1. Generate a 2D cartesian mesh for the entire domain.
2. Disintegrate the 2D channel profile into finite segments and determine the centroid and normal for each segment.
3. Track the solid-fluid interface using search algorithm and tag the nodes as fluid or solid nodes. Also find the normal distances for the interface nodes i.e. the fluid nodes in the vicinity of solid nodes.
4. Repeat the above two steps for the pressure, horizontal velocity and vertical velocity grids.
5. Apply the fourier transform to obtain the U_{in} in case of transient study.
6. Initialize the values for all parameters as zeros.
7. Initiate the computation by marching in time step:
    a) Swap the values of parameters with previous time step.
    b) Implement the boundary condition for the whole computational domain including the intercepted cells.
    c) Apply the discretized governing equations to predict the velocities for the entire domain.
    d) Again implement the boundary condition for the whole computational domain.
    e) Determine the divergence field for the predicted velocities ($\nabla \cdot V$). If zero return to step 7.a), otherwise proceed to the corrector loop
    f) Corrector loop:
        i. Determine p'.
        ii. Update the velocities and pressure using p'.
        iii. Implement boundary condition for the whole domain.
        iv. Determine $\nabla \cdot V$. If $\nabla \cdot V <$ tolerance limit, end the correction and go to step 7.a), otherwise continue with the correction.

g) Terminate when the required terminating condition is achieved.

The terminating condition for steady flow is reduction of the velocity differnce between consecutive time steps upto the prescribed tolerance limit and for transient the termination condition is the completion of the time cycle.

2.5 Constriction model and fluid properties

The model used for constriction in this study is similar to the model used by Moayeri and Zendehbudi [12] which is cosine. It is given by the following equation:

$$r = r_0 - 2h\left[(1 - cos(\frac{\pi(z - z_0)}{z_0}))\right], \quad 0 \leq z \leq z_0 \tag{2.13}$$

Here, r_0 is the half-depth of the arterial channel which is equal to 0.16 cm. It is also shown in figure 2.5.

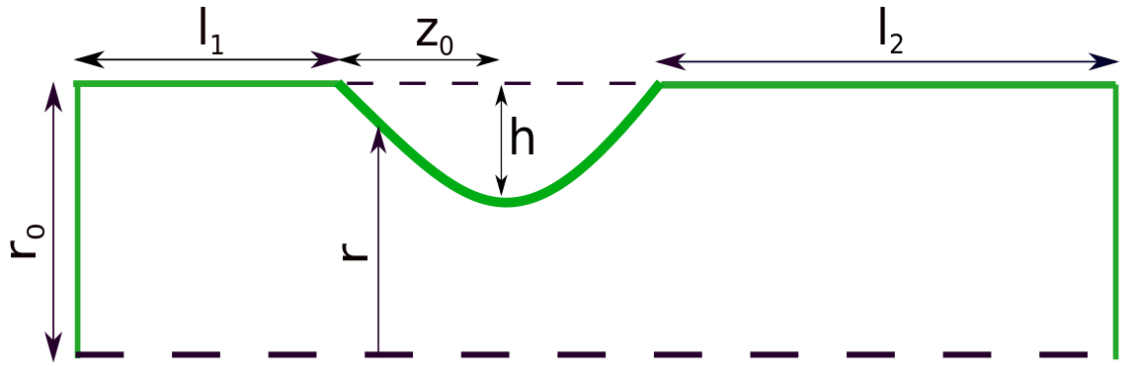

Figure 2.5: Constricted Channel

The fluid is assumed to have thermophysical properties of canine (dog) blood with density, ρ = 1054 kg/m^3 and dynamic viscosity, μ = 0.004 Pas. It is assumed to be homogenous, Newtonian an incompressible. It is similar to that used by Daly [10] and Moayeri and Zendehbudi [12]. The constriction model is assumed to have rigid wall and the wall distensibility effect is neglected. This can be of relevance in cases where the plaque deposition consists highly corbonated fats which makes the artery hard and stiff.

Chapter 3

Comparative Study

For testing and validating the technique, we have made two comparative studies: a) steady channel flow results are compared with the analytical solution; and b) backward step flow results are compared with the results of Gartling [20]. IBM is applied in both of these studies by maintaining the wall of the domain at a certain distance or offset from the computational grid which is shown in figure 3.1. The comparison has been described in the following sections.

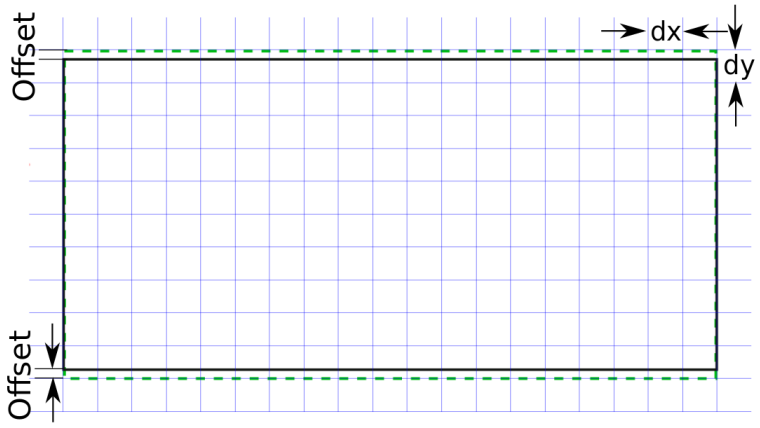

Figure 3.1: Offset in rectangular channel for the appliacation of IBM

3.1 Steady channel flow

The results of the numerical solution is obtained at a Reynolds number of 200. The CFL criteria used for the computation is 0.02. The analytical solution is obtained as a pure parabolic spatial flow profile with peak velocity at the centre and its value is 1.5 times of the average flow velocity. The quantitative comparison is as shown in table 3.1.

There are two sets of comparisons: a) the offset is 0.25dy which makes the interface closer to the solid node points; and b) the offset is 0.75dy which makes the interface closer to the fluid node points. The qualitative comparison of the numerical solution with analytical solution is given in figures 3.2 and 3.3

Table 3.1: RMSE for channel flow simulation

Grid	RMSE for 0.25dy offset	RMSE for 0.75dy offset
20×400	0.0020	0.0019
30×600	0.0014	0.0014
40×800	0.0011	0.0012

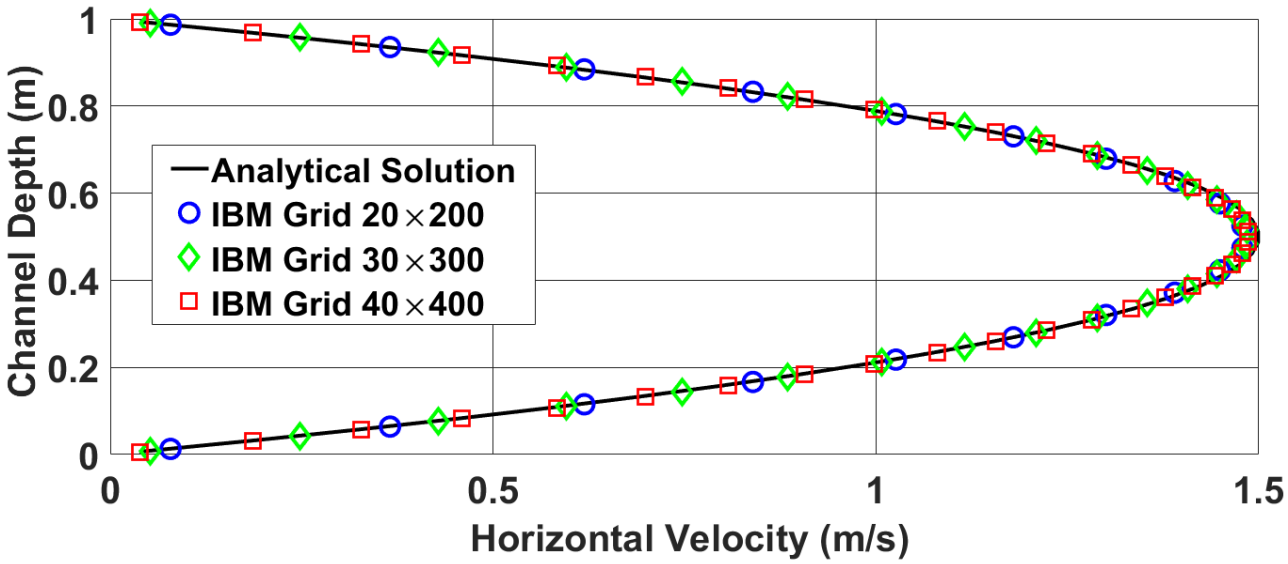

Figure 3.2: Variation of horizontal velocity with channel depth at offset of 0.25dy

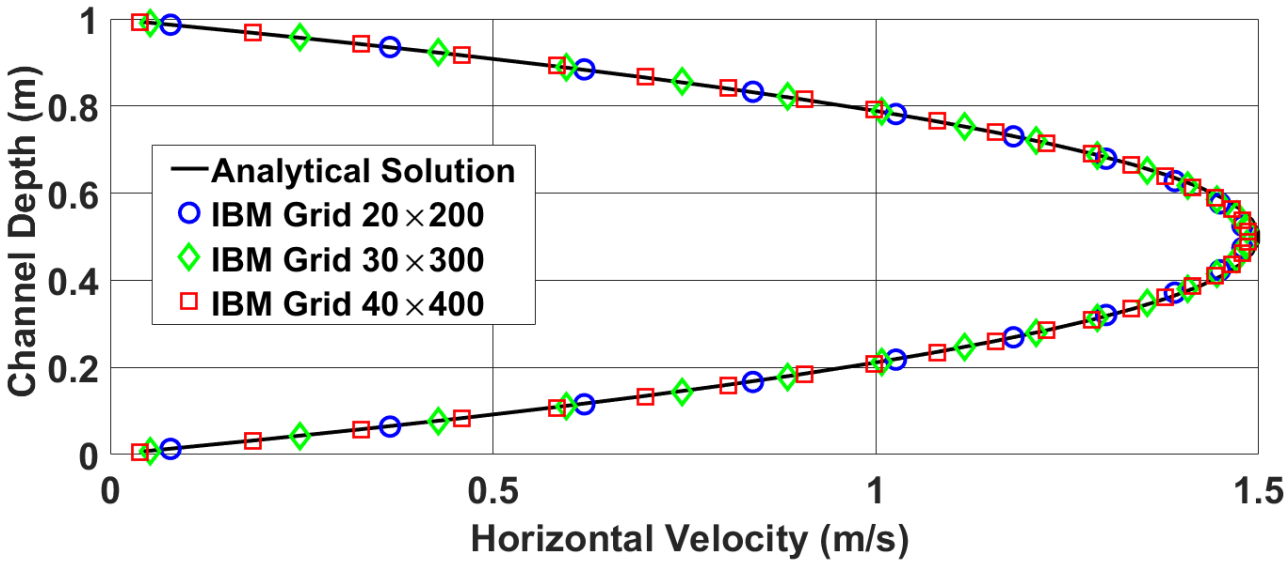

Figure 3.3: Variation of horizontal velocity with channel depth at offset of 0.75dy

As it can be seen in the table 3.1 the RMSE error recorded is to the order of 10^{-3}. So our scheme is successful in the simulation of numerical across a channel.

3.2 Backward Step flow

The backward step flow study is conducted at a Reynolds number of 800 to validate the results of our scheme with those of Gartling [20]. The inlet velocity profile for the flow is given in figure 2.4(b). The CFL criteria used for the computation is 0.02. The depth of the channel is 1m and the length is 25 times the depth. A parabolic spatial velocity profile is given at the top half of the inlet section of the computational domain. The qualitative comparison of the results of the current numerical scheme with the results published by Gartling [20] are as shown in the the figures 3.4, 3.5 and 3.6.

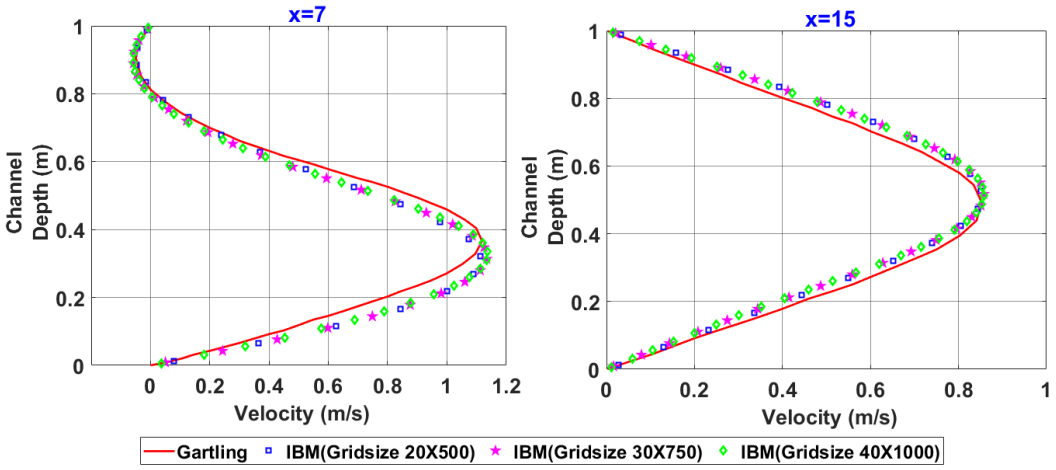

Figure 3.4: Comparison of horizontal velocity at x=7 and x=15

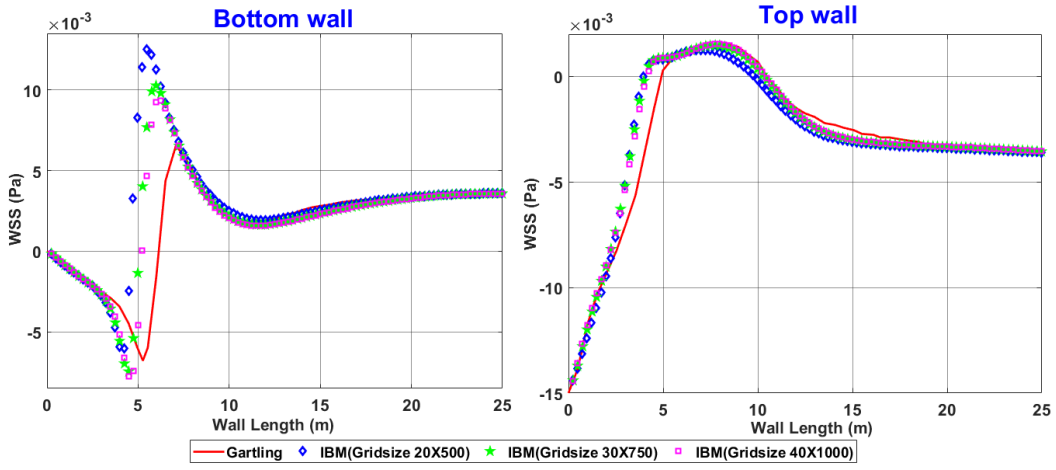

Figure 3.5: Comparison of wall shear stress at bottom and top wall

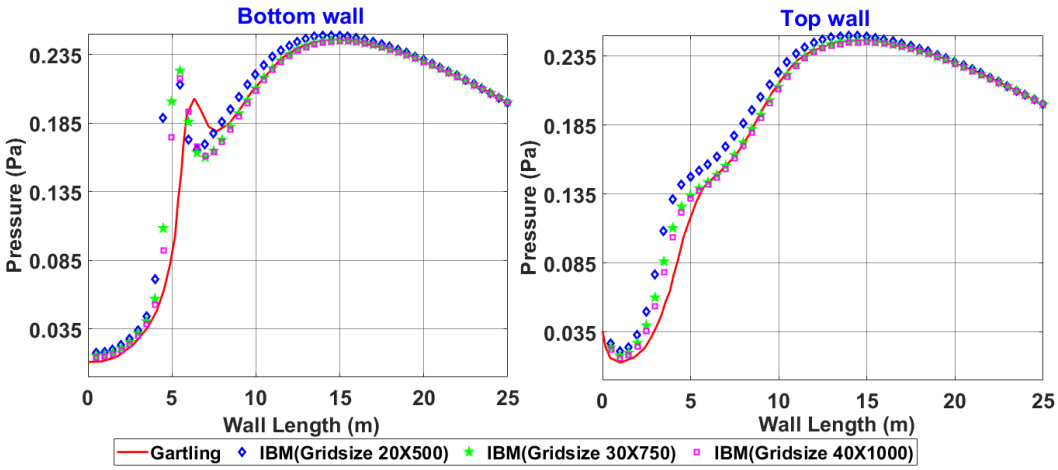

Figure 3.6: Comparison of wall pressure at bottom and top wall

The quantitative comparison of the separation zones have also been made and is shown in table 3.2.

Table 3.2: Size of lower and upper recirculation zone

Study	Lower Separation Zone Length	Upper Separation Point	Upper Reattachment Point
Gartling	5.69	4.79	10.48
IBM 20×500	4.60	4.00	9.80
IBM 30×750	5.07	4.10	10.33
IBM 40×1000	5.25	4.20	10.45

The results of the current numerical technique show good agreement with the results of Gartling on both qualitative and quantative terms with slight gap which is within the purview of numerical error. So our scheme has been successful in the simulation of flow across a backward step.

Chapter 4

Steady Flow Simulation

The Reynolds number used for the steady state simulation is 293.3. The CFL criteria used for the computation is 0.1174. The computational domain of the arterial channel can be divided into three main zones: a) initial development zone l_1, b) contriction zone $2z_0$ and the end development zone l_2. We have developed two different sets of results: one is for constriction length, $2z_0 = 5r_0$ and the other are for constriction length, $2z_0 = 10r_0$ whereas the initial development zone length, $l_1 = 20r_0$ and the end development zone, $l_1 = 30r_0$ are kept same for both cases. The computational grid is 30×825 for the short constriction case and 30×900 for the long constriction case. The inlet and exit of the computational domain are aligned with the cartesian coordinates whereas the wall is offset by 0.25dy as shown in figure 4.1.

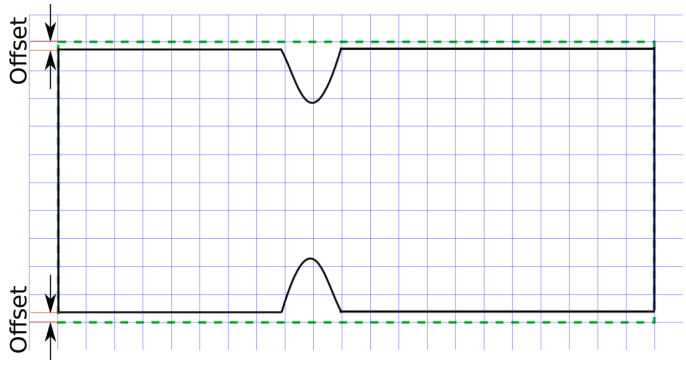

Figure 4.1: Offset in the constriction model

4.1 Short constriction length ($5r_0$)

There are three separate cases in this section: a) 0% constriction, b) 25% constriction, and c) 50% constriction. The % constriction represents the amount of area reduction. Since this study is conducted on channel the percentage of depth reduction will be equal to percentage of area reduction. The results of velocity and wall shear stress (WSS) comparisons of the three cases at four different positions in the channel from the begining of constriction are shown in figures 4.2 and 4.3 respectively.

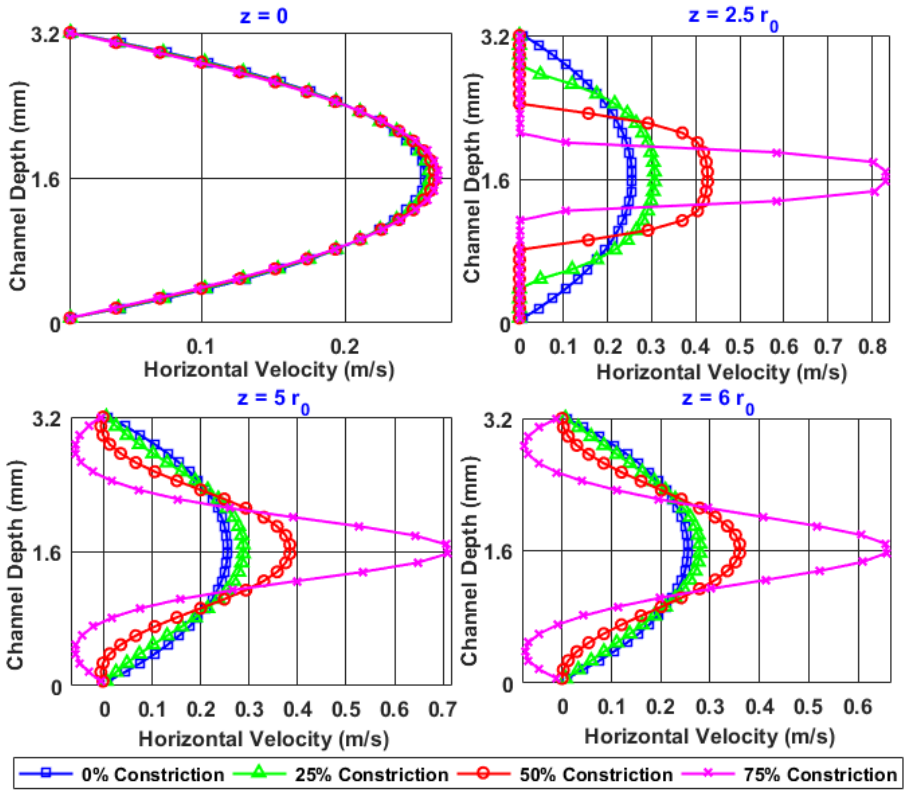

Figure 4.2: Velocity profiles for $2z_0=5r_0$ (The four different positions are taken with respect to the start of stenosis or constriction)

As the figures show with increasing constriction the velocity profiles become sharper. Even at the start of constriction the velocity profile is a little sharper for the constriction cases. At the centre of the constriction, a velocity value slightly less than the peak velocity is observed. The peak velocity is actually observed at a short length after the constriction centre. At the end of the constriction a slightly negative velocity is observed for the 50% and 75% constriction cases due to flow separation, but no negative velocity is observed for 25% constriction case. The negative velocity for the 50% and 75% constriction case continues for about $1.2r_0$ and $8r_0$ respectively after the constriction. After a length of about $10r_0$ for 25% case, $18r_0$ for 50% case and $24r_0$ for 75% case the velocity normalizes and becomes equal to the channel flow case.

The WSS variation with length show a trend similar to the results of Moayeri and Zendehbudi [12]. The peak WSS occurs before the centre of constriction for the constriction cases. There is a small segment of the wall where the WSS is negative which corresponds to the negative velocity. The WSS rises by approximately 7 times from 3.01 Pa at 25% constrcition to 20.3 Pa at 75% constriction. It shows that the growth in WSS if of higher degree than the growth in the size of constriction which could lead to severe biological problems.

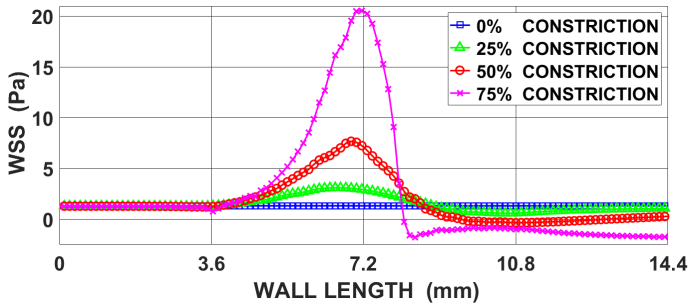

Figure 4.3: WSS for $2z_0=5r_0$(Wall length starts from $2r_0$ before constriction and ends at $2r_0$ after constriction)

The contour plots for the constriction cases are shown in figure 4.4. The total flow separation zone length observed for the 50% case was $2.2r_0$ and 75% case was $9.5r_0$. However no flow separation was observed in the 25% constriction case. The contour plots show a region of high pressure gradient at the constriction. The pressure gradient becomes higher for higher constriction (4.4). The p* denotes the scalar term in the governing equations which is p/ρ.

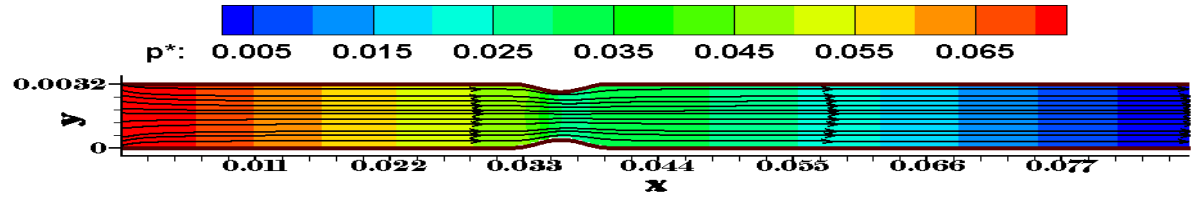

(a)

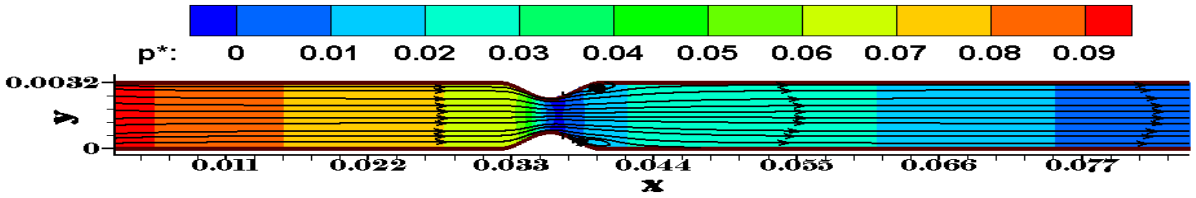

(b)

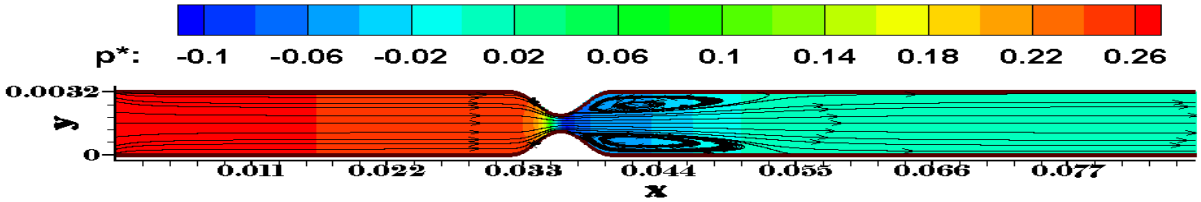

(c)

Figure 4.4: Pressure contours and streamline for: a) 25% Constriction; b) 50% Constriction; and c) 75% Constriction.

4.2 Long constriction length ($10r_0$)

The three separate cases are similar to the previous section. The results of velocity and wall shear stress (WSS) comparisons are shown in figures 4.5 and 4.6 respectively.

The results show a similar trend as observed in the previous section. No reversal zone is observed in the 25% and 50% constriction cases. However for the 75% constriction case the reversal zone length is approximately $10r_0$. The peak velocity is observed at about $0.2r_0$ to $0.25r_0$ after the centre of constriction for all the constriction cases. The velocity normalizes after $12r_0$, $18r_0$ and $22r_0$ in the 25%, 50% and 75% constriction case respectively.

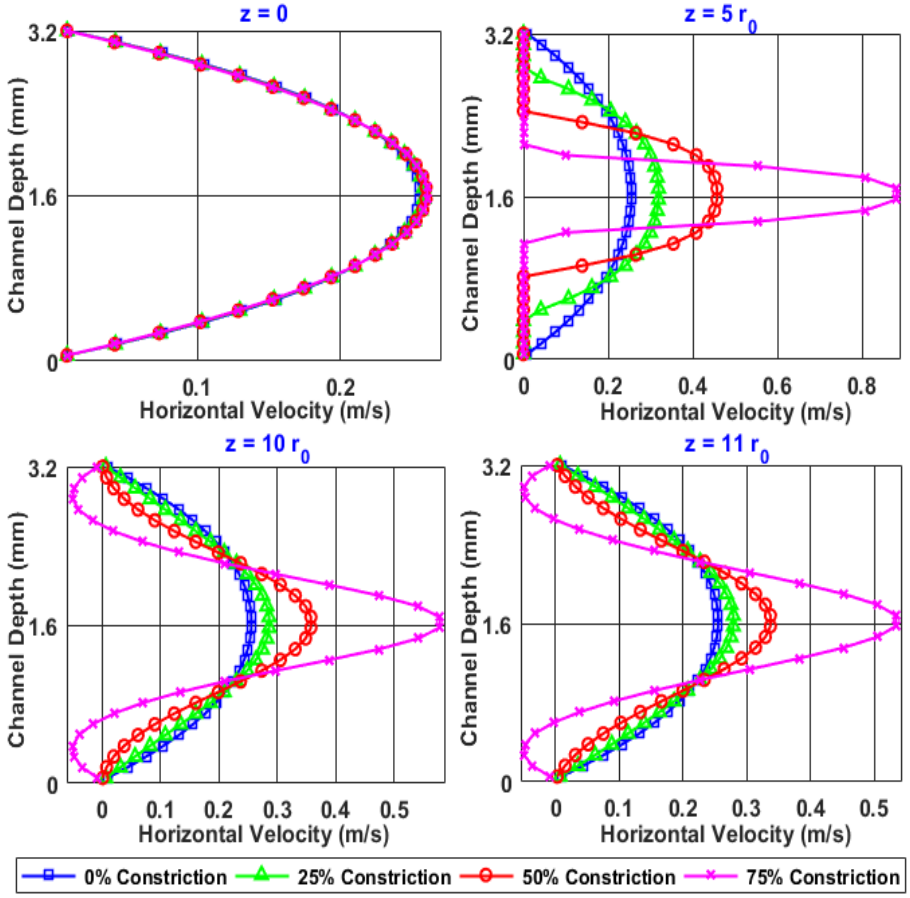

Figure 4.5: Velocity profiles for $2z_0$=$10r_0$

The WSS plot also shows a trend similar to the previous case. No negative WSS is observed for the 25% and 50% constriction cases as there is no negative velocity in this case. However some negative WSS is observed for the 75% constriction case. The peak value of WSS for the 50% constriction case and 75% constriction case is lower compared to the short constriction case. It shows that the length of the constriction also has effect on the severity of the stenosis. With longer length severity reduces.

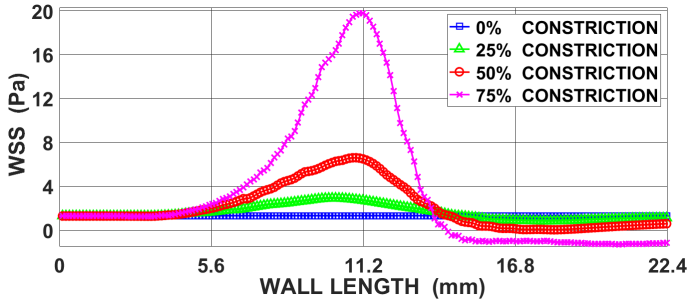

Figure 4.6: WSS for $2z_0$=$10r_0$(Wall length starts from $2r_0$ before constriction and ends at $2r_0$ after constriction)

The contour plots for the constriction cases are shown in figure 5.5. The contour plots show a region of high pressure gradient at the constriction similar to the trend in the previous section.

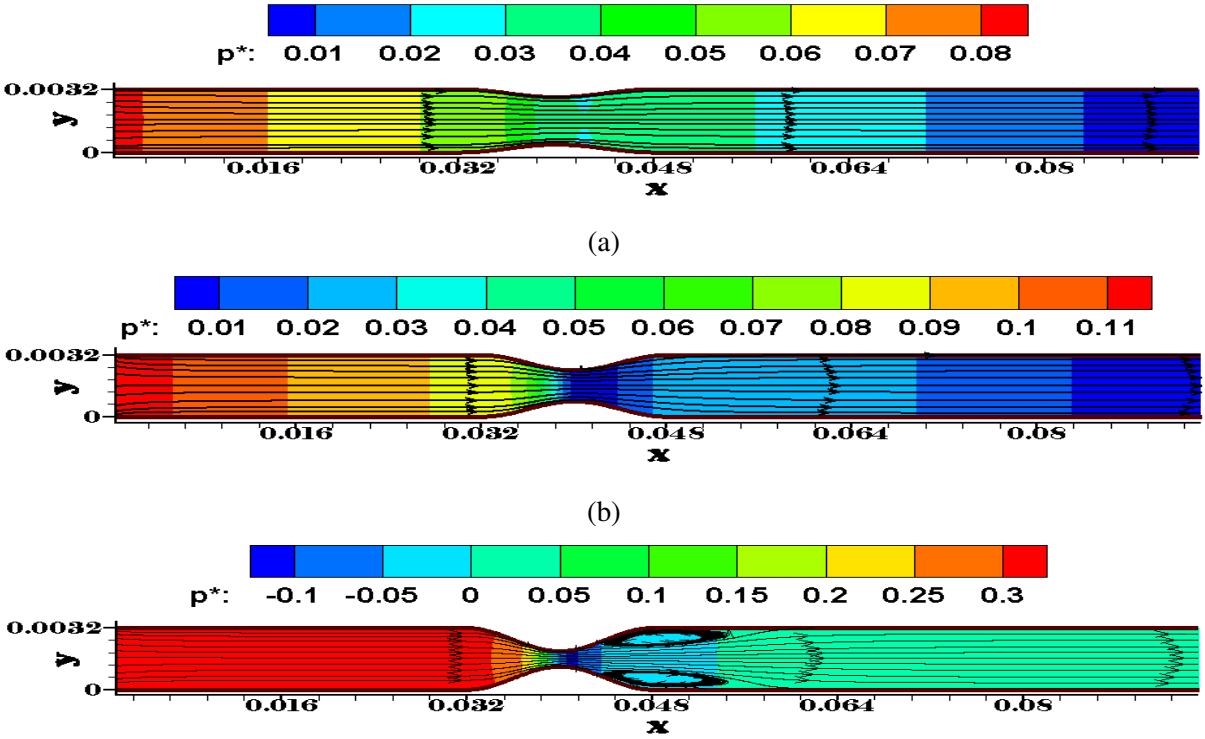

Figure 4.7: Pressure contours and streamline for: a) 25% Constriction; b) 50% Constriction; and c) 75% Constriction

4.3 Conclusions

The study of steady physiological flow has relevance for small arteries where Womerseley number is much less than 1. Generally the radius of these arteries is less than 1mm. The above

results show that with increase in constriction, turbulence in flow increases. This turbulence can cause eddies to form which can accelerate the process of plaque deposition. The WSS also increases with increase in constriction. This could be damaging to the endothelium as the exposure of the endothelium to this stress will be permanent [6].

Chapter 5

Unsteady Flow Simulation

The unsteady flow simulation is performed with the computational grid of 20×500 and the CFL criteria used for the computation is 0.0543. The lengths of the different segments of the domain are as follows: initial development zone length, $l_1 = 20r_0$; conctriction zone, $2z_0 = 5r_0$ and the end development zone, $l_1 = 30r_0$ The inlet velocity (U_{in}) used for the unsteady flow simulation is the physiological flow of canine femoral artery published by McDonald [3] (fig 5.1). The peak Reynolds number for the flow is 2006.8 for channel flow.

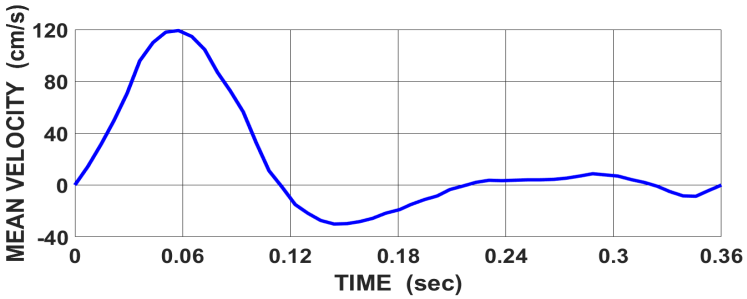

Figure 5.1: Mean velocity in canine femoral artery for a cardiac cycle

Figures 5.2 and 5.3 compares the velocity and wall shear stress respectively for various constrictions. The time period of one cycle of the flow is, T_0 = 0.36 seconds. The simulation is performed for only one cycle. The Womersely number for the flow is, α=3.43, so the velocity profiles of the flow are of Womerseley nature as shown in fig. 5.2.

The flow reversal begins at the end of systole i.e. $0.4T_0$ and continue for some period into dystole upto $0.6T_0$. The peak flow and the peak shear stress occurs a short time after the peak stenosis and so does the peak pressure gradient. It is to be noted that the peak wall shear stress (WSS) is almost 14 times that of peak WSS in case of steady flow with same constriction. The peak velocity is however only 5 times of the peak velocity in the steady case.

A continous occurence of low wall shear stress is observed in the wake of stenosis which could cause accumulation of cholestrol in that region as reported by Sako [5]. This accumulation worsens the ailment leading to more severe stenosis and that is a progression that leads to either death or surgery. Also the vertical acceleration of fluid in the wake of stenosis could

cause thrombus dislodgement if it gets out of phase with the motion of the distensible wall as reported by Daly [2].

The contour plots of pressure at different instances of time for the 25% constriction case are shown in figure 5.5. The flow behaviour is forward and normal during systole ($0.4T_0$). After that, flow reversal happens and eddies began to form as can be seen in figure 5.5c. The flow becomes normal again at $0.8T_0$. However, at the end, slight aberration is again visible. The contour plots show a region of high pressure gradient at the constriction which is similar to the trend in the steady flow case. The pressure gradient will become larger for higher constriction.

A phase lag of 60° is also observed between pressure gradient and fluid flow (5.5a) which is consistent with the results reported by Womerseley [4] (5.4).

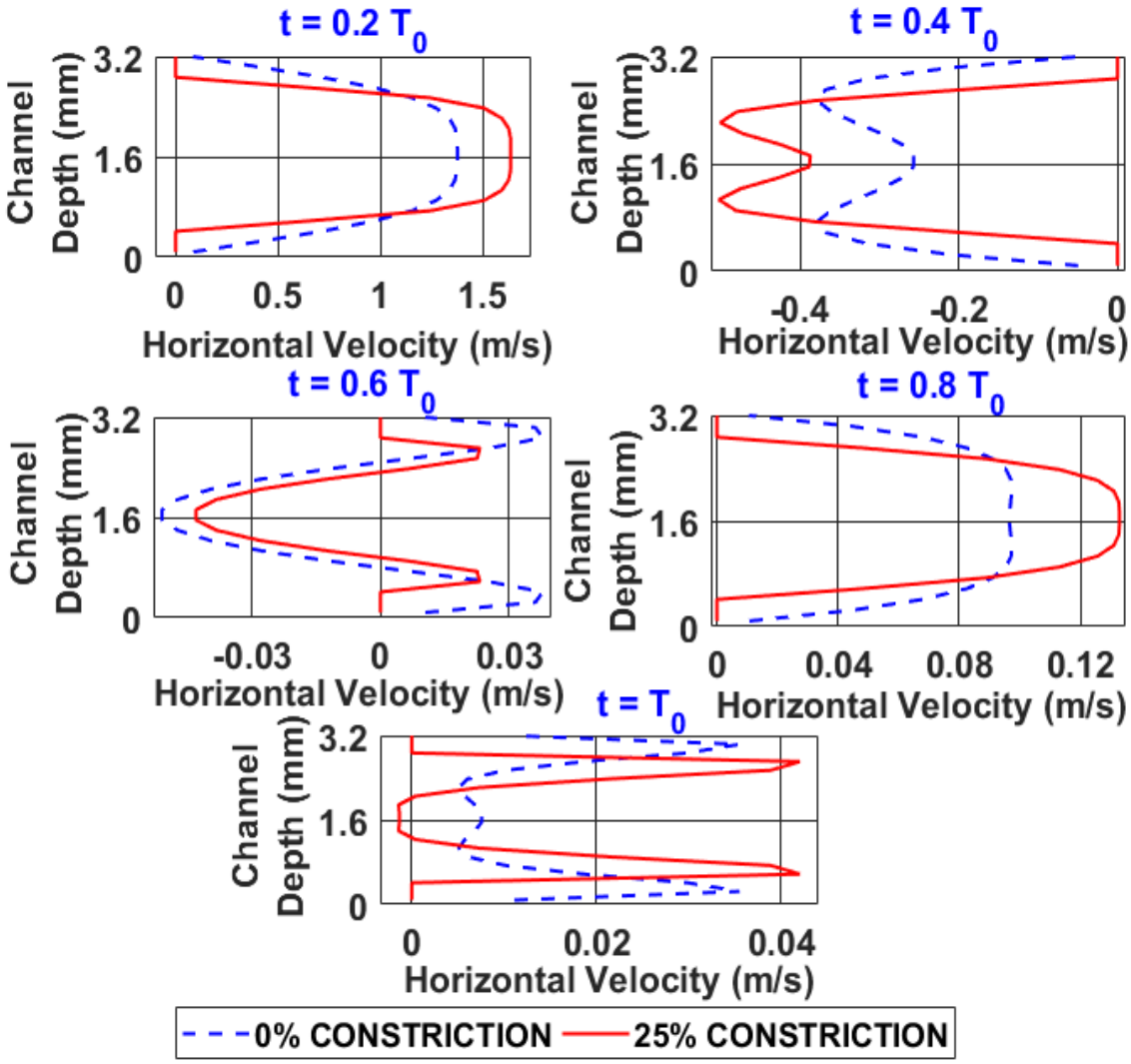

Figure 5.2: Horizontal velocity at various constrictions and at various time steps at the center of constriction.

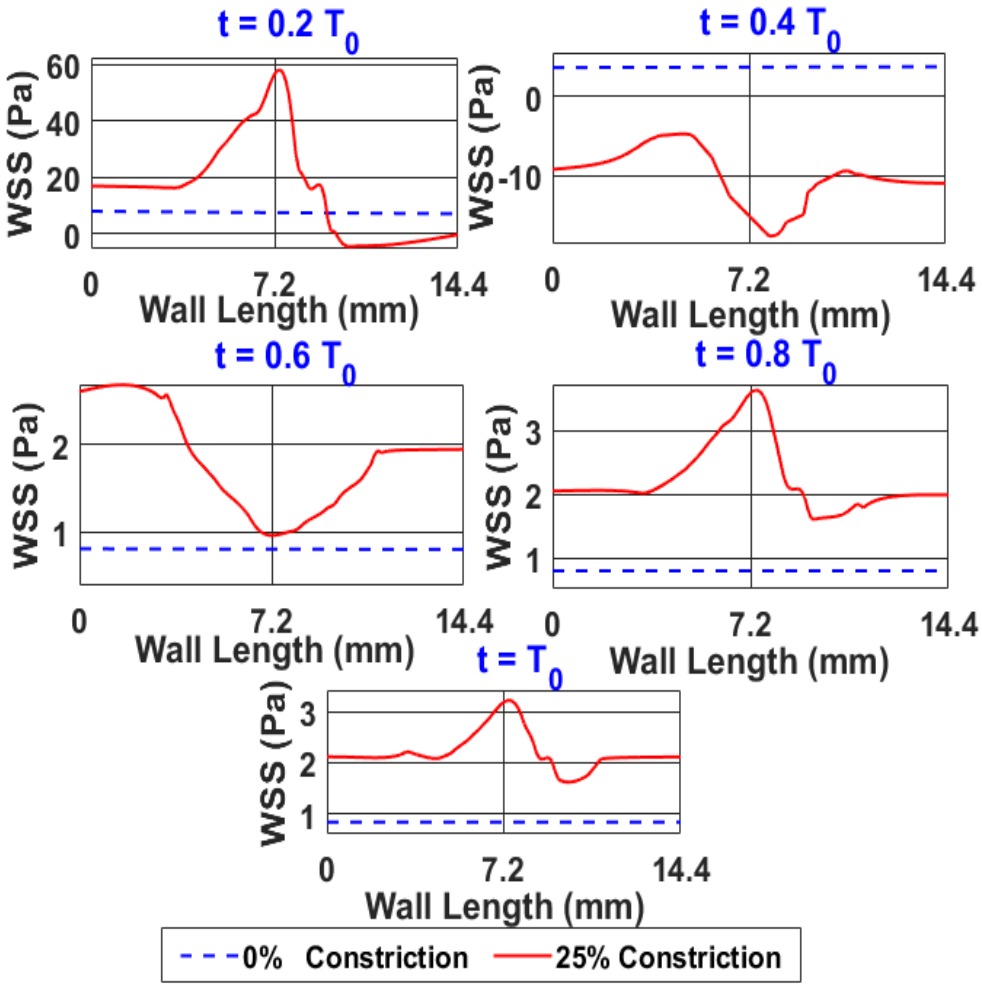

Figure 5.3: Wall shear stress at various constrictions and at various time steps along the wall length (Wall length starts from $2r_0$ before constriction and ends at $2r_0$ after constriction)

Figure 5.4: Variation of phase lag with Womerseley number.

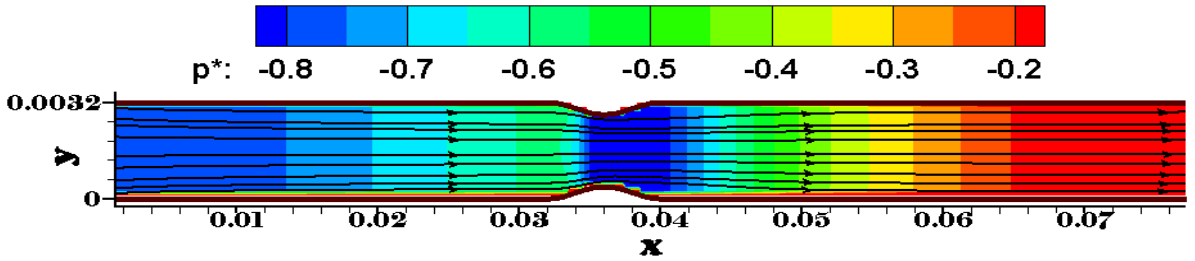

(a)

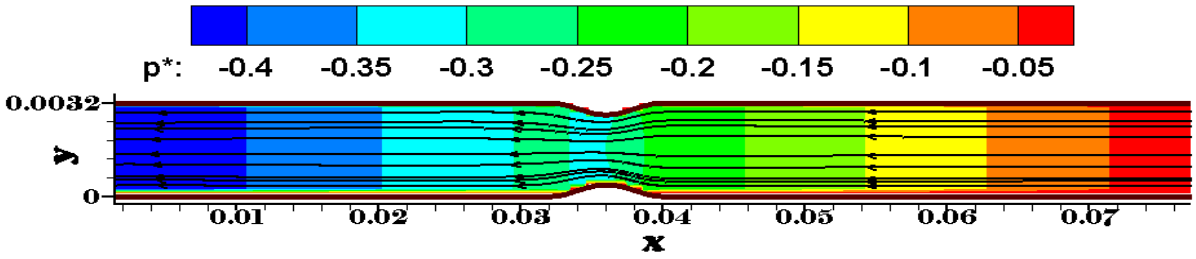

(b)

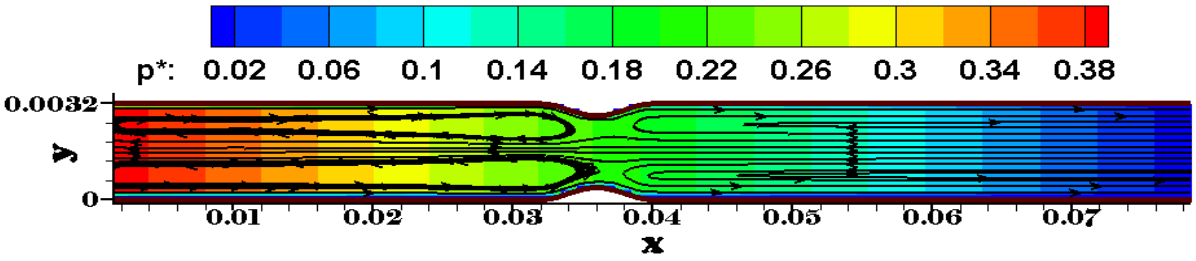

(c)

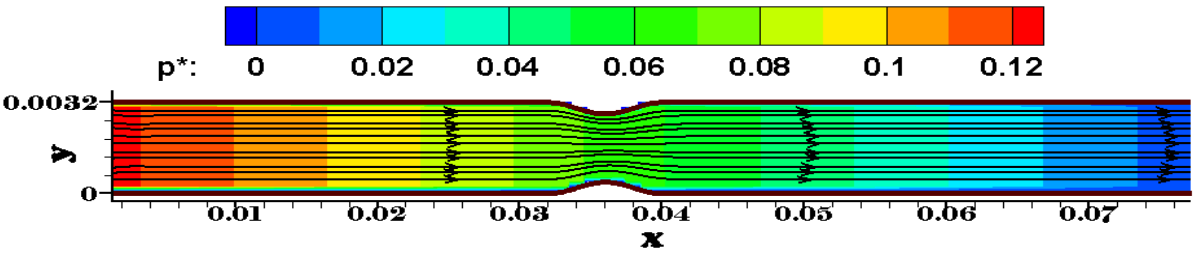

(d)

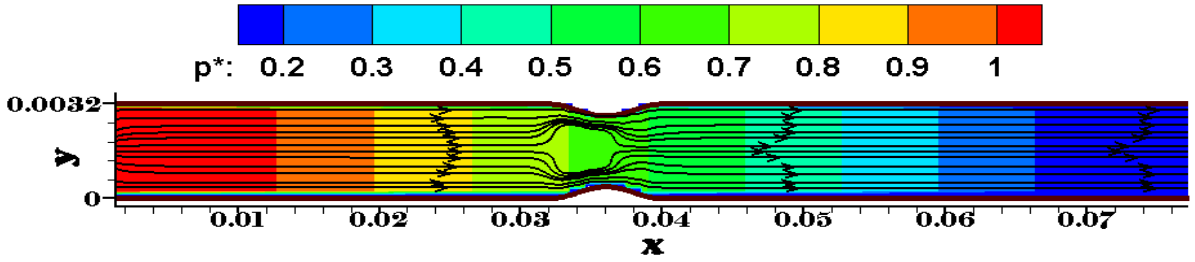

(e)

Figure 5.5: Pressure contours and streamline at: a) t= $0.2T_0$; b) t= $0.4T_0$; c) t= $0.6T_0$; d) t= $0.8T_0$; and e) t= T_0

Chapter 6

Conclusions

The present study is a novel application of the IBM to study physiological flow in 2D stenosed artery. The application of the IBM to implement the boundary values or boundary conditions simplified the process of computation for the complex curved profile of the stenosis. It aslo opened up the possibility of the application of simple FDM based fluid flow solver like SOLA to be applied in a complex geomtery. The simplicity of the computation provided by the above scheme is unparalleled. The use of SOLA solver has also eliminated the computational expense of interpolating the pressure boundary conditions. No amount of skewness or asymmetry was observed in the results which can happen in cases of unstructured mesh generation. The results of the steady and unsteady flow simulation are very much in line with the results reported by previous researchers and hence validate the accuracy of the technique. The effect of the constrictions in arteries and pulsatile flow on the fluid behaviour are studied and it was observed that primarily secondary flows are in direct correlation with the WSS.

6.1 Scope for future work

1. The study could be extended to distensible walls using appropriate FSI coupling model. The use of IBM will make it easier to incorporate the moving boundary as there is no need to change the mesh structure regularly.

2. The study could be extended for non-Newtonian fluids using appropriate non-Newtonian flow model such as Casson's mobel.

3. The study could be extended to complex 3D patient specific models which includes branches and protrusions and other complexities.

4. Other numerical techniques such as NIM (Nodal Integral Method) could be used to reduce the time expenditure. Although the algorithm is a little complex for these techniques but they can generate results faster.

5. Realistic boundary conditions such as RCR, impedance,etc to simulate real hemodynamic environment could be implemented.

6. Better iterative techniques such as TDMA, bi-conjugate method, etc could be used to speed up the corrective process.

7. The use of MPI could also help in speeding up the simulation process. The current simulation was entirely performed on a single processor. The use of MPI can reduce the computational time significantly.

Bibliography

[1] M. Kumar, S. Roy, and M. S. Ali, "An efficient immersed boundary algorithm for simulation of flows in curved and moving geometries," *Computers and Fluids*, vol. 129, pp. 159–178, 2016.

[2] B. J. Daly, "A numerical study of pulsatile flow through stenosed canine femoral arteries," *Journal of Biomechanics*, vol. 9, pp. 465–475, 1976.

[3] D. A. McDonald, "The relation of pulsatile pressure to flow in arteries," *Journal of Physiology*, vol. 127, pp. 533–552, 1955.

[4] J. R. Womersley, "Method for the calculation of velocity, rate of flow and viscous drag in arteries when the pressure gradient is known," *Journal of Physiology*, vol. 127, pp. 553–563, 1955.

[5] Y. Sako, "Effects of turbulent blood flow and hypertension on experimental atherosclerosis," *Journal of American Medical Association*, vol. 179, pp. 36–40, 1962.

[6] D. L. Fry, "Acute vascular endothelial changes associated with increased blood velocity gradients," *Circulation Research*, vol. 22, pp. 165–197, 1968.

[7] D. Young and J. H. Forrester, "Flow through a converging-diverging tube and its implications in occlusive vascular disease- I," *Journal of Biomechanics*, vol. 3, pp. 297–305, 1970.

[8] D. Young and F. Tsai, "Flow characteristics in models of arterial stenoses-I. Steady Flow," *Journal of Biomechanics*, vol. 6, pp. 395–410, 1973.

[9] D. F. Young and F. Y. Tsai, "Flow characteristics in models of arterial stenoses - ii. Unsteady Flow," *Journal of Biomechanics*, vol. 6, pp. 547–559, 1973.

[10] B. J. Daly, "4th International conference on numerical methods in fluid dynamics," in *Lecture Notes in Physics*, vol. 35, (Berlin, Germany), pp. 117–135, Springer, 1974.

[11] L. Vanderschuren, C. Tu, M. Deville, and L. Dheur, "Finite element simulation of pulsatile flow through arterial stenosis," *Journal of Biomechanics*, vol. 25(10), pp. 1141–1152, 1992.

[12] B. J. Zendehbudi and M. S. Moayeri, "Comparison of physiological and simple pulsatile flows through stenosed arteries," *Journal of Biomechanics*, vol. 32, pp. 959–965, 1999.

[13] I. E. Vignon and C. Taylor, "Outflow boundary conditions for one-dimensional finite element modeling of blood flow and pressure waves in arteries," *Wave Motion*, vol. 39, pp. 361–374, 2004.

[14] C. S. Peskin, "Flow patterns around heart valves: a numerical method," *Journal of Computational Physics*, vol. 10, pp. 252–271, 1972.

[15] R. Mittal and G. Iaccarino, "Immersed boundary methods," *Annual Reviews of Fluid Mechanics*, vol. 37, pp. 239–261, 2005.

[16] C. W. Hirt, B. D. Nichols, and N. C. Romero, "Sola: A numerical solution algorithm for transient fluid flows," *Technical Report LA- 5852*, 1975.

[17] E. W. Merrill and G. A. Pelletier, "Viscosity of human blood: transition from newtonian to non-newtonian," *Journal of Applied Physiology*, vol. 23, pp. 178–182, 1967.

[18] K. Anupindi, Y. Delorme, D. A. Shetty, and S. H. Frankel, "A novel multiblock immersed boundary method for large eddy simulation of complex arterial hemodynamics," *Journal of Computational Physics*, vol. 254, pp. 200–218, 2013.

[19] K. Muralidhar and T. Sundarajan, "Computational fluid flow and heat transfer," Narosa Publishing House, 2008.

[20] D. K. Gartling, "A test problem for outflow boundary conditions: flow over a backward-facing step," *International Journal for Numerical methods in fluids*, vol. 11, pp. 953–967, 1990.